AGU PUBLICATIONS

JGR

Journal of Geophysical Research: Space Physics

RESEARCH ARTICLE
10.1002/2014JA020343

This article is a companion to *Richard et al.* [2015] doi:10.1002/2013JA019706.

Key Points:
- Empirical production rates were derived for various superthermal electron fluxes
- Electron and ion density discrepancies are not due to primary ion overproduction
- Primary production is modeled without magnetospheric electron flux attenuation

Correspondence to:
T. E. Cravens,
cravens@ku.edu

Citation:
Richard, M. S., et al. (2015), An empirical approach to modeling ion production rates in Titan's ionosphere II: Ion production rates on the nightside, *J. Geophys. Res. Space Physics*, *120*, 1281–1298, doi:10.1002/2014JA020343.

Received 27 JUN 2014
Accepted 28 DEC 2014
Accepted article online 6 JAN 2015
Published online 3 FEB 2015

An empirical approach to modeling ion production rates in Titan's ionosphere II: Ion production rates on the nightside

M. S. Richard[1,2], T. E. Cravens[1], C. Wylie[1], D. Webb[1], Q. Chediak[1], K. Mandt[3], J. H. Waite Jr.[3], A. Rymer[4], C. Bertucci[5], A. Wellbrock[6,7], A. Windsor[2], and A. J. Coates[6,7]

[1]Department of Physics and Astronomy, University of Kansas, Lawrence, Kansas, USA, [2]Department of Physics and Astronomy, Benedictine College, Atchison, Kansas, USA, [3]Space Science and Engineering Division, Southwest Research Institute, San Antonio, Texas, USA, [4]Johns Hopkins University Applied Physics Laboratory, Laurel, Maryland, USA, [5]Institute for Astronomy and Space Physics, COCICET/University of Buenos Aires, Buenos Aires, Argentina, [6]Mullard Space Science Laboratory, University College London, London, UK, [7]Centre for Planetary Sciences, University College London/Birkbeck, London, UK

Abstract Ionization of neutrals by precipitating electrons and ions is the main source of Titan's nightside ionosphere. This paper has two goals: (1) characterization of the role of electron impact ionization on the nightside ionosphere for different magnetospheric conditions and (2) presentation of empirical ion production rates determined using densities measured by the Cassini Ion and Neutral Mass Spectrometer on the nightside. The ionosphere between 1000 and 1400 km is emphasized. We adopt electron fluxes measured by the Cassini Plasma Spectrometer-Electron Spectrometer and the Magnetospheric Imaging Instrument as classified by Rymer et al. (2009). The current paper follows an earlier paper (Paper I), in which we investigated sources of Titan's dayside ionosphere and demonstrated that the photoionization process is well understood. The current paper (Paper II) demonstrates that modeled and empirical ionization rates on the nightside are in agreement with an electron precipitation source above 1100 km. Ion production rate profiles appropriate for different Saturnian magnetospheric conditions, as outlined by Rymer et al., are constructed for various magnetic field topologies. Empirical production rate profiles are generated for deep nightside flybys of Titan. The results also suggest that at lower altitudes (below 1100 km) another source, such as ion precipitation, is probably needed.

1. Introduction

As a result of ionization of its neutral atmosphere [*Waite et al.*, 2005, 2007; *Vuitton et al.*, 2006, 2007; *Magee et al.*, 2009], Titan is surrounded by an ionosphere whose density peaks at altitudes between 900 and 1200 km [*Wahlund et al.*, 2005; *Young et al.*, 2005; *Keller et al.*, 1992; *Gan et al.*, 1992; *Cravens et al.*, 2004, 2005, 2008, 2009a, 2009b; *Galand et al.*, 1999; *Banaskiewicz et al.*, 2000; *Molina-Cuberos et al.*, 2001; *Lilensten et al.*, 2005a, 2005b; *Agren et al.*, 2007; *Kliore et al.*, 2008] (see recent review by *Galand et al.* [2014]). The ionosphere has been detected using the radio occultation technique by both the Voyager 1 and Cassini spacecraft [*Bird et al.*, 1997; *Kliore et al.*, 2008; *Cravens et al.*, 2009a]. In situ electron density measurements were first made during the Cassini Ta encounter [*Wahlund et al.*, 2005], and ion density measurements were first made by the Cassini Ion and Neutral Mass Spectrometer (INMS) during the T5 nightside flyby of Titan [*Cravens et al.*, 2006].

Titan's location in Saturn's magnetosphere determines the superthermal electron populations that exist and can precipitate along magnetic field lines into the ionosphere [*Carbary and Krimigis*, 1982; *Arridge et al.*, 2006, 2008; *Coates et al.*, 2007a; *Carbary et al.*, 2007; *Bertucci et al.*, 2008; *Rymer et al.*, 2009; *Sergis et al.*, 2009]. As Titan lacks a significant intrinsic magnetic field [*Hartle et al.*, 1982; *Neubauer et al.*, 1984], the magnetic field line topology is dictated by the draping of Saturnian magnetic field lines around Titan (cf. review by *Sittler et al.* [2009]). *Rymer et al.* [2009] classified outer magnetospheric electron populations based on Titan's location using data from the Cassini Plasma Spectrometer-Electron Spectrometer (CAPS-ELS) and the Magnetospheric Imaging Instrument (MIMI). Four classes of spectra were identified: (1) plasma sheet, (2) lobe like, (3) magnetosheath, and (4) bimodal. Related to this, *Kliore et al.* [2011] emphasized the large variability in electron densities in Titan's ionosphere measured by the Cassini Radio Science Subsystem indicating wide variations in the superthermal electron population of the same classification.

Models of the ionosphere have shown that energetic magnetospheric electron and ion precipitation can also take place and contribute to the ionization rate and atmospheric heating, particularly at lower altitudes [cf. *Galand et al*., 2014; *Agren et al*., 2007; *Cravens et al*., 2008, 2009a, 2009b; *Gronoff et al*., 2009a, 2009b; *Sillanpaa and Johnson*, 2013]. Ionization sources on the nightside for the T5 encounter of Titan were discussed by *Agren et al*. [2007], *Cravens et al*. [2009b], *Robertson et al*. [2009], and *Gronoff et al*. [2009b]. One conclusion was that the flux of magnetospheric electrons precipitating into the atmosphere needs to be reduced by a factor of 10 in order to reproduce the electron densities measured by the RPWS-LP (Radio Plasma Wave Science-Langmuir Probe) instruments aboard the Cassini spacecraft. The current paper will come to different conclusions.

Snowden et al. [2013] and *Gan et al*. [1993] demonstrated that "erosion" of Saturnian magnetic flux tubes (i.e., depletion of the electron content) caught up in Titan's ionosphere can result in such attenuation of incident superthermal electron fluxes. *Gronoff et al*. [2009b] specifically examined the ion production of N_2^+, N^+, and CH_4^+ using their TransTitan model [*Gronoff et al*., 2009a] in order to consider effects of magnetic field line geometry on the ionization processes. This was similar to the work done by *Cravens et al*. [2009b]. In situ magnetic field measurements [e.g., *Neubauer et al*., 1984; *Bertucci et al*., 2009] combined with post-Cassini global MHD and hybrid models [*Ma et al*., 2009; *Ledvina et al*., 2012] demonstrated that the magnetic field line topology is complex, particularly at lower altitudes. The magnetic fields produced by global models do not generally agree with magnetometer data below 1300 km or so [*Ulusen et al*., 2010].

Chemical models incorporating neutral and/or ion chemistry have been created to explain observed ion densities at Titan [*Keller et al*., 1992; *Krasnopolsky*, 2009; *Lavvas et al*., 2008a, 2008b; *Robertson et al*., 2009; *Vuitton et al*., 2007, 2008; *Westlake et al*., 2012; *Wilson and Atreya*, 2004]. *Robertson et al*. [2009] used a steady state photochemical model of the ion-neutral chemistry that, coupled with a photoionization and two-stream code, generated the primary (those caused by photoionization) and secondary (those caused by electron impact ionization) ion production rates and calculated ion densities as a function of altitude as was done in the model of *Keller et al*. [1992]. The model of Robertson et al. did not contain information about negative ion chemistry which could be important in the lower ionosphere [*Vuitton et al*., 2008; *Ågren et al*., 2012; *Shebanits et al*., 2013; *Wellbrock et al*., 2013; *Vigren et al*., 2014] or ion transport effects which limit the applicability of this model above 1400 km or to very long lived ion species, where ion transport becomes nonnegligible [*Ma et al*., 2006; *Cui et al*., 2010].

The current paper will use the two-stream method to handle suprathermal electron transport in the atmosphere. This method was originally used to calculate electron fluxes in the terrestrial ionosphere [*Nagy and Banks*, 1970] and has been used in models of both the energetics and composition of Titan's ionosphere [*Gan et al*., 1992; *Cravens et al*., 2009b; *Robertson et al*., 2009; *Snowden et al*., 2013]. This method derives from a gyrotropic distribution function averaged over a gyroperiod [cf. *Schunk and Nagy*, 2009]. As photoelectrons and magnetospheric electrons move along field lines, they may scatter in a new direction or ionize a neutral thus creating another electron. This secondary electron must then also be tracked along the field line. Monte Carlo simulations have shown that considering only two streams, one up and one down [cf. *Schunk and Nagy*, 2009, and references therein], is usually sufficient in the ionosphere. Once "primary" ion production rates are determined (due to solar radiation, particle precipitation, etc.), chemistry alters the ion composition, as discussed in Paper I for the dayside.

First, comparisons between nightside INMS measurements and modeled ion densities will be made for a few passes (similar to what was done for the dayside in Paper I) [*Richard et al*., 2015]. Empirical ion production rates will be constructed from INMS data using the methods of Paper I. Next, generic ion production profiles for the canonical cases discussed by *Rymer et al*. [2009] will be generated for three magnetic field line topologies (horizontal (nested), parabolic, and radial fields). The goal of this endeavor is to produce ion production rate profiles to enable future modeling efforts to combine the solar ion production profiles with the ion production caused by magnetospheric electrons when Titan is located in an area of Saturn's magnetosphere characterized by Rymer et al. to predict the ion production and density profiles for future flybys of Titan.

2. Methodology

Electron impact ionization appears to be the main in situ ionization source of the nightside of Titan above ≈ 1000 km [cf. *Agren et al*., 2007; *Cravens et al*., 2009a, 2009b; *Robertson et al*., 2009]. In this section we provide more information on the methods used.

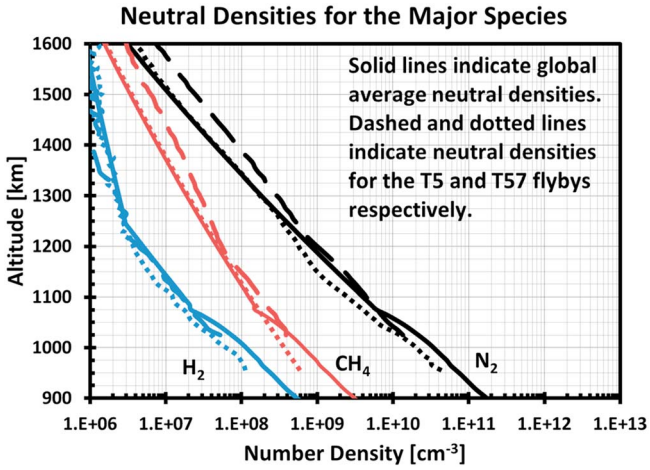

Figure 1. Number density of major neutral species derived from INMS measurements for the global average (solid lines), T5 (dashed lines), and T57 (dotted lines) flybys of Titan. N_2, CH_4, and H_2 are indicated by the black, red, and blue lines, respectively. The number densities have been multiplied by a factor of 3.15 in this figure in order to account for a potential recalibration of the INMS instrument.

2.1. Neutral Densities

The neutral densities required in the model are those measured by INMS for N_2, CH_4, and H_2. Figure 1 shows densities for ingress of the T5 and T57 flybys. The densities all include a factor of 3.15 increase associated with the recalibration of the instrument [cf. *Westlake et al*., 2012; *Mandt et al*., 2012]. Continuing calibration efforts (J. H. Waite Jr., manuscript in preparation, 2015) indicate that the INMS closed source neutral density calibration factor might be closer to 2.5 and that the factor for open source ion measurements might be a factor of 1.5 higher than values used in this paper (which are consistent with Mandt et al.). As our empirical ion production rates are obtained from the product of neutral and ion densities, the actual values could potentially be 20% larger. This 20% modification is within statistical error bars of the data, and the conclusions of the paper are unaffected.

Neutral densities for the remaining 35 neutral species in the model are determined using the mixing ratio profiles of *Krasnopolsky* [2009] or *Lavvas et al*. [2011] for the case of CH_2NH, anchored to mixing ratios reported by *Magee et al*. [2009], *Cui et al*. [2009], and *Robertson et al*. [2009]. This method is described in detail in Paper I [*Richard et al*., 2015].

Another set of neutral density profiles was used in our determination of "generic" ion production rates associated with precipitation of different magnetospheric electron populations as outlined by *Rymer et al*. [2009]. The global average model of the neutral atmosphere discussed in Paper I (Richard et al.) was implemented and was based on INMS [*Magee et al*., 2009] data from 40 Titan flybys and on the Huygens Atmospheric Structure Instrument data below 960 km [*Fulchignoni et al*., 2005], from which profiles of N_2, CH_4, and H_2 are derived (Figure 1).

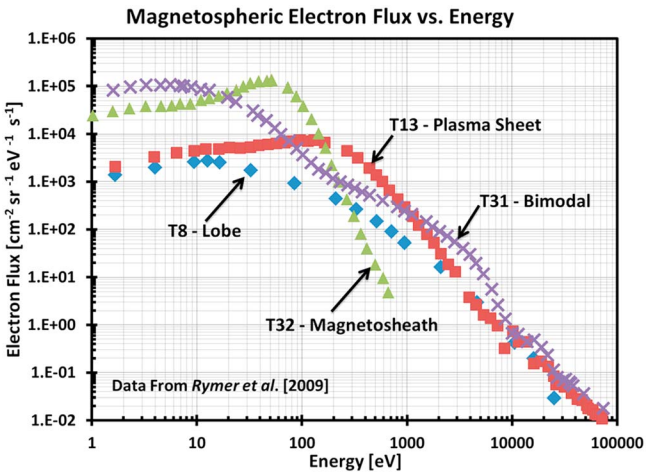

Figure 2. Superthermal electron fluxes measured by the Cassini CAPS and MIMI instruments in Saturn's outer magnetosphere plotted against energy for the four magnetospheric plasma environments presented by *Rymer et al*. [2009].

2.2. Two-Stream Equations for Suprathermal Electron Flux

Electron fluxes as a function of energy and ion production rates are calculated by solving two-stream equations [*Nagy and Banks*, 1970; *Schunk and Nagy*, 2009] using Saturn's magnetospheric electron flux (i.e., Figure 2). Discussion of the application of this method to Titan can be found in *Gan et al*. [1992, 1993], *Cravens et al*. [2009b], and *Richard et al*. [2011]. Given the complexity of the magnetic field topology and at least partial disagreement of global plasma/field models (e.g., MHD) with magnetometer data, we follow the lead of Gan et al. and adopt parabolic field lines in addition to radial field lines. The apex altitude determines the

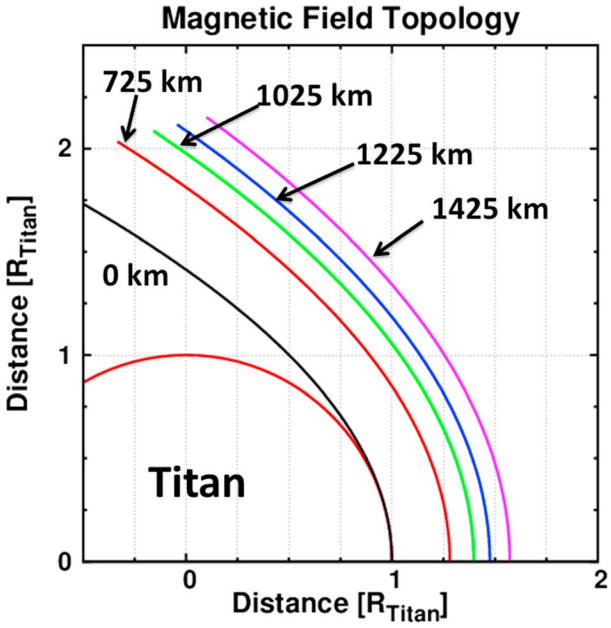

Figure 3. Parabolic magnetic field line topology used in the model. The apex altitude of each field line is indicated on the graph.

dip angle of the field lines at ionospheric altitudes. For example, for T5 putting the apex at the surface results in field lines that have a dip angle of about 45° near 1100 km, in agreement with Cassini magnetometer data shown by *Richard et al.* [2011] and discussed by *Cravens et al.* [2009b]. These papers show that the magnetic field vectors have large radial and horizontal components throughout the T5 flyby. Parabolic field lines are shown in Figure 3.

We now briefly describe how the inelastic electron impact cross sections, σ, for a species j with an electron of energy E are calculated using the parametric formula of *Green and Dutta* [1967]. For the differential ionization cross section the expression developed by *Green and Sawada* [1972] is implemented. Elastic electron differential cross sections are calculated from the values of *Trajmar et al.* [1983] and *Solomon et al.* [1988] and have been integrated by *Gan et al.* [1992] in order to obtain the backscatter probabilities and the elastic cross section as a function of energy for electron-N_2 collisions. The sum of vibrational excitations of molecular nitrogen through inelastic collisions was taken from *Porter et al.* [1976]. For the cross section of the A, B, B′, C, a, a′, and W states the revised cross sections of *Cartwright et al.* [1977] by *Trajmar et al.* [1983] were used. The cross sections of the b′ and $^1\Pi_u$ were obtained from *Zipf and McLaughlin* [1978]. The sum of the Rydberg states was derived by normalizing the values from *Green and Stolarski* [1972] to the total dissociation cross sections of Zipf and McLaughlin when they are added to the cross sections of the b′ and $^1\Pi_u$ states.

The ionization cross sections of *Tabata et al.* [2006] and *Itikawa* [2006] are used in the current work. Differential elastic electron impact cross sections of methane have been taken from the theoretical work of *Jain* [1986] over energy ranges from 0.1–1 eV, 2.5–20 eV, and 30–400 eV. Backscattering probabilities, integrated cross sections, and momentum transfer cross sections have been calculated from these results. The results of *Tanaka et al.* [1983] are used for the differential cross sections above 2 eV. Measurements are provided between 3 and 20 eV, and extrapolations are used for energies above 20 eV. Vibrational excitation cross sections at 2 eV are taken from those of *Rohr* [1980], and for energies below 2 eV cross sections are used from the measurements of *Sohn et al.* [1983].

The electronic excitation cross sections of methane are derived from the measurements of *Vuskovic and Trajmar* [1983]. Rotational excitation cross sections for methane are taken from the theoretical work of *Jain and Thompson* [1983] and multiplied by a factor of 2 in order to bring their work into better agreement with measurements of *Muller et al.* [1985], *Brescansin et al.* [1989], and *Shimamura* [1983]. Ionization cross sections for CH_4 are taken from the work of *Straub et al.* [1997] as revised by *Lindsay and Mangan* [2003] and reviewed by *Liu and Shemansky* [2006].

The two-stream equations require the downward flux at the upper boundary. We use a variety of downward electron fluxes based on magnetospheric electron fluxes measured by Cassini in the nearby Saturnian magnetosphere. For example, in modeling electron precipitation for T5, *Cravens et al.* [2009b] used the CAPS-ELS fluxes which are reproduced here in Figure 4 with a factor of 3.15 increase in the neutral densities to account for INMS recalibration. Also shown are the CAPS-ELS electron fluxes measured at 1200 km, near the ionospheric peak, and our calculated fluxes are within 5–20% of the CAPS-ELS fluxes up to energies of 200 eV using parabolic magnetic field lines anchored at the surface of Titan (Figure 3). Between 200 and 1000 eV the CAPS-ELS data are at the one-count level, which is the statistical error bound of the instrument, and our model differs from these fluxes by as much as a factor of 2, which could be the result of modest

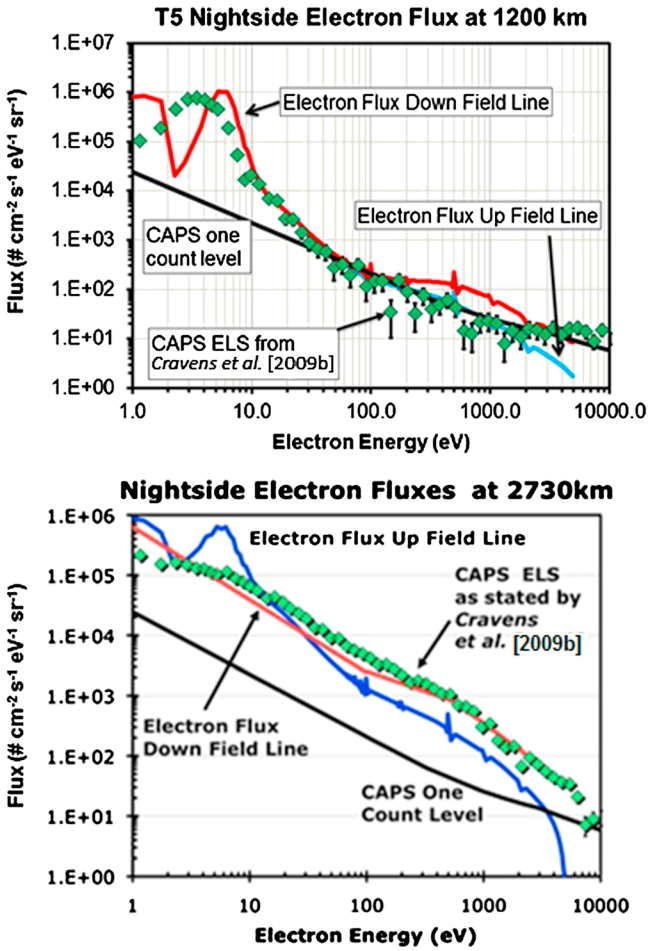

Figure 4. Suprathermal magnetospheric electron fluxes measured by CAPS during the T5 encounter as reported by *Cravens et al.* [2009b] at 1200 km (above) and 2730 km (below). The downward flux comes from suprathermal electron transport along the field line from the magnetosphere to the ionosphere. These CAPS-ELS fluxes for T5 were adopted as the boundary condition for the two-stream code, and model fluxes are also shown. The upward electron fluxes appearing at higher energies are calculated from the model and are the results of backscattering and at lower energies are escaping secondary electrons produced by ionization deeper in the atmosphere.

attenuation of the electron fluxes [*Snowden et al.*, 2013]. The CAPS-ELS instrument was pointed in the ram direction, and as a result the pitch angle of the instrument was approximately 90° [cf. *Cravens et al.*, 2009b].

2.3. Ion Chemistry and Empirical Modeling

The photochemical model we use here was described in Paper I [*Richard et al.*, 2015] and was derived from the earlier photochemical models of *Keller et al.* [1992, 1998], *Cravens et al.* [2004], and *Robertson et al.* [2009]. This time-independent model does not include ion transport between altitudes or horizontal locations as a result of bulk plasma flow, an assumption valid below ≈ 1350 km [*Ma et al.*, 2006, 2009; *Cravens et al.*, 2010]. In addition to adopting the primary ion production rates, the model includes a large number of ion-neutral and electron-ion dissociative recombination chemical reactions. Reaction rate coefficients are taken from *Keller et al.* [1992, 1998], *Anicich* [2003], *Anicich and McEwan* [1997], *Cravens et al.* [2005], *Vuitton et al.* [2006, 2007], *McEwan and Anicich* [2007], *Edwards et al.* [2008], *Zabka et al.* [2009], *Robertson et al.* [2009], and *Westlake et al.* [2012]. We use 10 km intervals between 725 and 2715 km but only show results below about 1700 km.

As discussed in Paper I (Richard et al.), a measured density of N_2^+ cannot be determined by INMS ion measurements because $HCNH^+$ is a more abundant mass 28 species due to ion-neutral chemistry. The overwhelming majority of N_2^+ on the nightside is produced by electron impact ionization, and about 60–85% of this N_2^+ is lost via chemical reactions with methane, producing CH_3^+. A small amount of CH_3^+ is produced by dissociative ionization of methane. Roughly 90–99% of the CH_3^+ is lost via reaction with methane to produce CH_4^+. Thus, the production of CH_3^+ serves as a good indicator (or proxy) of the primary production of N_2^+.

CH_3^+ densities from the model are compared with the densities measured by INMS in Figure 5. This illustrates that the production rate of N_2^+ (the major source of CH_3^+) in the model is reasonable. The drop in ion densities near 1200 km will be discussed later. In the companion Paper 1, an empirical production rate of N_2^+ was derived from densities of CH_3^+ and CH_4 measured by INMS by means of a simple two-reaction model and the assumption of photochemical equilibrium (which is valid below ≈ 1350 [*Ma et al.*, 2006, 2009; *Cravens et al.*, 2010]). The main loss process for CH_3^+ is through reaction with methane. Not quite all of N_2^+ reacts with CH_4 to produce CH_3^+, so the full photochemical model was used to derive a branching ratio of CH_3^+ produced to the total amount of N_2^+ produced (Figure 6). This ratio only varies about 20% over the extent of the ionosphere. Using this model-derived branching ratio, the derived empirical production rate (reasonable

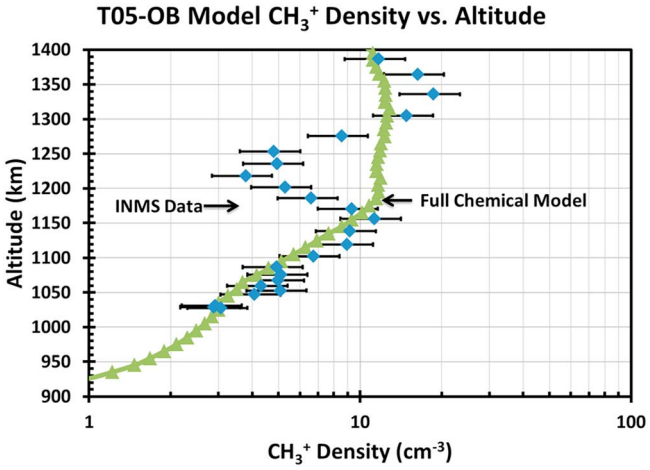

Figure 5. CH_3^+ density produced by the full photochemical model (green triangles) using the full T5 magnetospheric electron flux measured by CAPS-ELS [*Cravens et al.*, 2009b] as an input (Figure 4) compared to INMS data from the T5-Outbound flyby of Titan. INMS data are indicated by the blue diamonds. This model uses the magnetic field topology of a single parabola anchored at the surface of Titan to simulate a curved field line with a large radial component.

to within 40%) of N_2^+ determined by setting the production rate of N_2^+ equal to the loss rate from the reaction between CH_3^+ and CH_4 is given by

$$\text{Production}_{N_2^+} = \frac{k_{CH_3^+,\,CH_4}\left[CH_3^+\right]_{INMS}[CH_4]_{INMS}}{\text{Branching Ratio}} \quad (1)$$

Similarly, an empirical primary production rate of CH_4^+ due to ionization of CH_4 can be derived. Note that about 90% of the CH_4^+ loss is due to reaction with methane to produce CH_5^+ but that other sources (besides primary ionization) exist (e.g., CH_4 reacting with H_2^+, H^+, or N^+). Therefore, this production rate is the loss rate of CH_4^+ (via reaction with CH_4) modified by a branching ratio (Figure 6) to account for alternative production pathways (see Paper I (Richard et al.)). The empirical primary production rate (including the model-derived branching ratio) is

$$\text{Production}_{CH_4^+} = \frac{k_{CH_4^+,CH_4}[CH_4]_{INMS}\left[CH_4^+\right]_{INMS}}{\text{Branching Ratio}} \quad (2)$$

3. Verification of Nightside Ion Production Rates via Simple Empirical Methods

In this section, the model ionization rates (from electron impact) are compared with the empirical production rates, just as was done in Paper 1 for solar radiation. We start with data from the T5 flyby, as this case has been previously discussed in the literature [i.e., *Cravens et al.*, 2009b; *Robertson et al.*, 2009; *Gronoff et al.*, 2009b; *Agren et al.*, 2007], and then we discuss the T57 flyby. For the T5 case, Titan was in the plasma sheet and T57 corresponds to what *Rymer et al.* [2009] call "bimodal" magnetospheric electron distributions. We find that overall, the model production rates of the primary ion species are in reasonable agreement with the production rates derived from INMS density measurements, as will be discussed below for the canonical cases of Rymer et al. (lobe like, plasma sheet, bimodal, and magnetosheath) and for three magnetic field line topologies (radial, single parabola, and nested parabolas simulating horizontal field lines).

3.1. T5: Plasma Sheet Electron Populations

The T5 flyby of Titan occurred on the deep nightside of Titan, and the Cassini Orbiter reached a closest approach altitude of 1027 km where the solar zenith angle was 137°. The neutral density profiles we used to analyze this pass were shown in Figure 1. Magnetometer data from the T5 encounter indicate that the dip angle of the magnetic field during the entire outbound leg of the T5 encounter was approximately 45° [*Cravens et al.*, 2009b; *Ulusen et al.*, 2010]. Using a parabolic magnetic field line anchored at the surface generates a field line dip angle in agreement with these observations between 1000 and 1400 km. The magnetospheric electron fluxes used as inputs for this case were discussed earlier (i.e., the plasma sheet case shown in Figure 4).

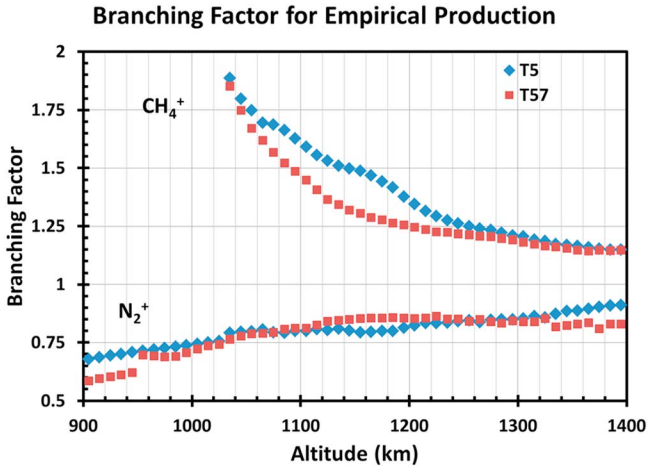

Figure 6. Branching ratio used to adjust the production rate of N_2^+ and CH_4^+ derived from the simple two-reaction model using INMS data for the outbound leg of the T5 and T57 flybys. This is the ratio of the production rate of CH_3^+ to N_2^+ (below) and of the primary production of CH_4^+ to the total production of CH_4^+ from the full photochemical model (above).

Figure 5 shows the CH_3^+ densities produced by the full photochemical model, and the model CH_3^+ densities are in good agreement with densities measured by INMS to within 20% for altitudes below 1160 km and above 1280 km. Between 1160 and 1275 km INMS and modeled CH_3^+ densities differ by about a factor of 2. This feature was noticed by both *Agren et al.* [2007] and *Cravens et al.* [2009b]. Cravens et al. demonstrated that the CAPS-ELS 4 eV electron flux, corresponding to secondary electrons, correlates well with the INMS density of CH_5^+, the product of the chemical reaction between CH_4^+ and methane, with a noticeable dip between 155 and 205 s after closest approach corresponding to altitudes of 1140 and 1220 km, respectively. Cravens et al. also noted that the density profiles of longer-lived ions (such as $HCNH^+$) do not exhibit such a profound drop in density at these altitudes. As the drop in density was only prevalent in shorter-lived ion species, Cravens et al. concluded that the production rate of ions, and hence the magnetospheric electron flux at the end of the flux tube connected to this region, was passing through more of the neutral atmosphere and was being depleted of its electron content [*Gronoff et al.*, 2009b; *Snowden et al.*, 2013]. This effect has been noted in several previous works [*Gan et al.*, 1992; *Agren et al.*, 2007; *Cravens et al.*, 2009b; *Ma et al.*, 2006, 2009; *Snowden et al.*, 2013]. *Cui et al.* [2010] suggested that transport from the dayside can also contribute to the densities of long-lived ions on the nightside.

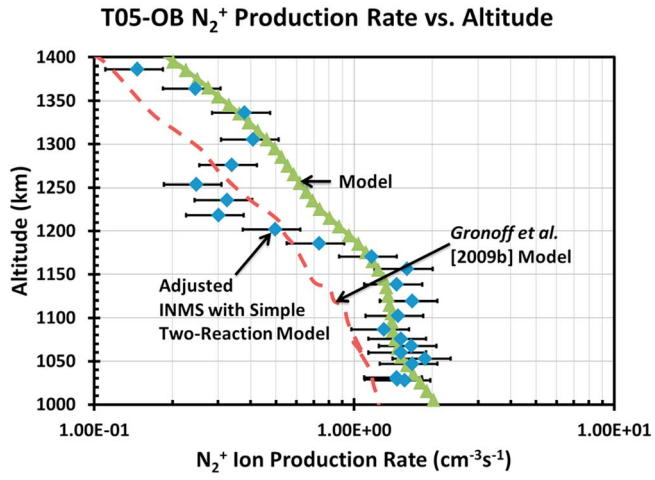

Figure 7. Modeled electron impact production rates of N_2^+ (green triangles) compared to the production rate of N_2^+ derived from INMS data using a simple two-reaction model adjusted by dividing the loss rate of CH_3^+ via reaction with methane by the branching ratio shown in Figure 6 (blue diamonds) for the outbound leg of the T5 flyby of Titan. The modeled production rates of *Gronoff et al.* [2009b] for a radial field line with flux attenuation are also shown (red dashes). A single parabolic field line anchored at the surface of Titan is used for the magnetic field line topology.

Although some depletion of the incident electron flux is apparently needed near 1200 km as discussed by *Gan et al.* [1992] and *Snowden et al.* [2013], at other altitudes the model agrees very well with INMS data. This indicates that overall for T5, the magnetospheric electron flux tube content appears to be depleted less than originally thought. This has significant consequences for our understanding of Titan's interaction with Saturn's magnetosphere. Earlier modelers [*Agren et al.*, 2007; *Cravens et al.*, 2009b] concluded that the overabundance of ions in chemical models was the result of using incident electron fluxes that were too large and thus the incident fluxes needed to be reduced by a factor between 8 and 10. This conclusion was the result of the lack of a recent recalibration of the neutral density profile and a focus on modeled total ion and electron

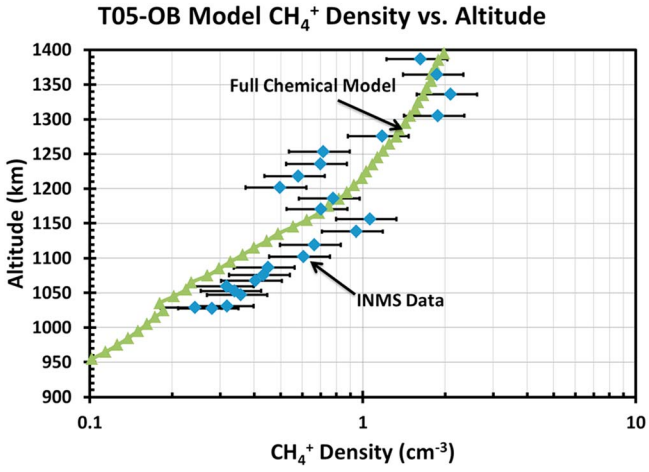

Figure 8. CH_4^+ density produced with the full photochemical model (green triangles) compared to INMS data (blue diamonds) from the T5-Outbound flyby of Titan. A single parabolic field line anchored at the surface of Titan is used for the magnetic field line topology.

densities, instead of examining individual ion species. As will be shown below, our current model also produces electron densities that are too high, but we think that the explanation (as discussed in Paper 1) is missing loss processes for major ion species (but not for CH_3^+), as occurs on the dayside. This will be discussed further later in the paper.

Next, we use CH_3^+ and CH_4 densities measured by INMS to obtain empirical N_2^+ production rates (methods discussed earlier and in Paper 1), which are shown in Figure 7 and compared with the two-stream model with the full T5 CAPS-ELS magnetospheric electron fluxes as input. The agreement between this model and the CAPS-ELS measurement and the model of *Gronoff et al.* [2009b] for their radial field line with attenuation is within 10–20% near the ionospheric peak with the exception of the "bite-out" feature between 1140 and 1220 km. At higher altitudes the discrepancy between our model and the model of Gronoff et al. increases due to our use of a parabolic instead of radial field line. This, in conjunction with the agreement between modeled and measured CH_3^+ densities, suggests that the two-stream model is producing adequate amounts of N_2^+ for the measured inputs.

The above methods were also applied to T5 for CH_4 ionization producing CH_4^+. Figure 8 shows the CH_4^+ densities from the full model compared with INMS densities. Again, the agreement is good overall, but the bite out is not reproduced by the model. Empirical ion production rates derived from INMS data are shown in Figure 9.

CH_4^+ production rates modeled using only magnetospheric electron impact ionization with the two-stream code and those derived empirically from INMS data agree between 1350 and 1200 km but are a factor of 2 lower between 1150 and 1000 km. However, this model's production rate is found to be in agreement with the radial case presented by *Gronoff et al.* [2009b] with a value of 0.04 $cm^{-3}\,s^{-1}$ between 1100 and 1000 km.

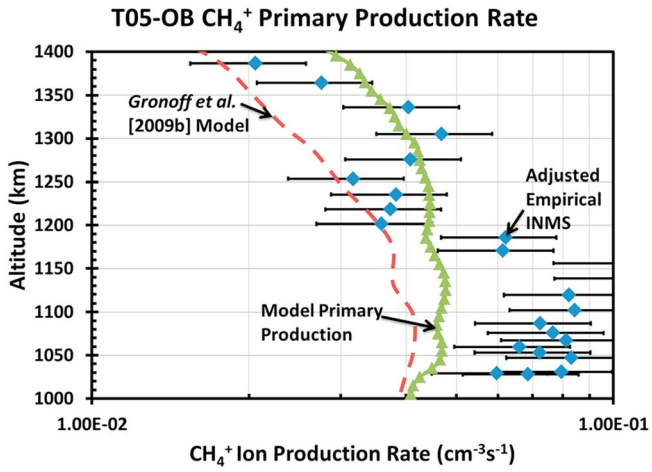

Figure 9. Shown here are modeled production rates (green triangles) of CH_4^+ compared to the empirical production rate of CH_4^+ derived from INMS data (blue diamonds) using the simple two-reaction chemical model for the T5-Outbound flyby of Titan and adjusted by dividing the loss rate of CH_4^+ via reaction with methane by the branching ratio shown in Figure 6. The modeled production rates of *Gronoff et al.* [2009b] for a radial field line with flux attenuation are also shown (red dashes).

3.2. T57: Bimodal Electron Populations

The T57 flyby of Titan occurred on 22 June 2009, and the spacecraft reached a closest approach altitude of 955 km. During the inbound leg the solar zenith angle went from 165° at an altitude of nearly 2000 km to 128° at closest approach, indicating that this is an entirely nightside situation. *Rymer et al.* [2009] classified the magnetospheric electron flux for this pass as a bimodal case (Figure 10).

For T57 we compare our calculated electron fluxes with fluxes measured by

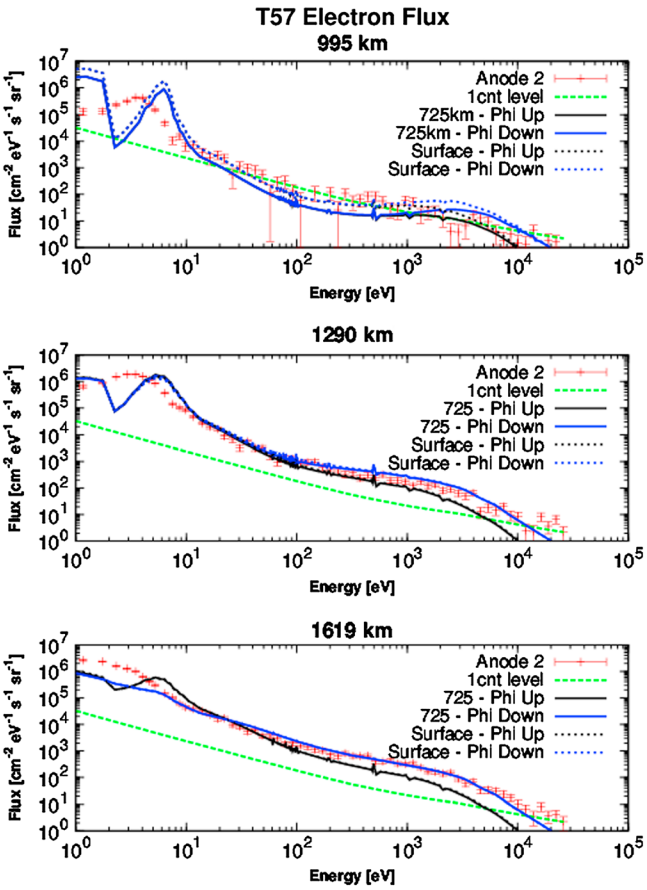

Figure 10. Comparisons between modeled electron fluxes and those measured by CAPS during the T57 encounter at (top) 995 km, (middle) 1290 km, and (bottom) 1619 km. Measurements taken by CAPS-ELS anode 2 are shown in red; modeled fluxes up (black) and down (blue) are shown for parabolic field lines anchored at 725 km (solid) and the surface of Titan (dashed). The CAPS-ELS one-count level is shown with a green line.

CAPS-ELS anode 2 at several altitudes and for different model cases (Figure 10). Results from several CAPS-ELS anodes (i.e., different directions) are shown. Note that anodes 3–6 point in or near the ram direction and see negative ions (or traces) [e.g., *Coates et al*., 2007b; *Wellbrock et al*., 2013] as well as electrons, so we will not comment on these. Out of the remaining anodes, anode 2 is least affected by spacecraft obscuration effects [*Lewis et al*., 2008] so we compare our results with measurements made by anode 2. Throughout the flyby the CAPS pitch angle was near 90° as was the case for the T5 flyby.

The following observations can be made by examining Figure 10. At 995 km only the more energetic electrons can penetrate the atmosphere, although locally produced secondary electrons at low energies (0–30 eV) are also present. Assuming a negative spacecraft potential between 2 and 3 eV would improve the model's agreement with the data for 10 eV electrons. The model's maximum electron flux above 1100 km near 10 eV (secondary electrons from primary electron impact ionization) is in reasonable agreement with measurements at higher altitudes, but at 995 km the model flux is somewhat too high, suggesting some possible attenuation (factor of 2–3) of the precipitation magnetospheric electron fluxes. For energies between about 20 eV and 300 eV the model fluxes along a surface-anchored parabolic magnetic field agree better with the CAPS data than those modeled using a parabolic field anchored at 725 km, which are too low by a factor of 2 or so. At 1064 km both model cases compare well with data, although model fluxes are somewhat too high near 5–10 eV and too low for energies above 1 keV (though the CAPS fluxes are close to the one-count level there). But the more draped 725 km magnetic field parabola gives somewhat better agreement overall. At 1163 km and higher for T57, both models agree rather well with the measured fluxes, although are maybe somewhat too large for energies greater than 1 keV or so.

Magnetometer data (Figure 11) show (C. Bertucci, private communication, 2012) that the magnetic field line topology for T57 has both radial and horizontal (parallel to the surface of Titan) components near the ionospheric peak. Near closest approach (between 950 and 1000 km), the magnetic field exhibits the strongest radial components with a magnitude of 75% of the total field magnitude. Between 1000 and 1100 km the radial component gradually diminishes to 25% of the total field's magnitude and the horizontal component increases. We ran the model with three different magnetic field line topologies (nested, single parabola anchored at the surface, and single parabola anchored at 725 km). The nested case represents completely horizontal field lines at all altitudes "sampled." The parabola anchored at the surface has field lines with a 45° angle with respect to Titan near 1200 km, and the parabola anchored at 725 km has a larger horizontal field component near 1200 km.

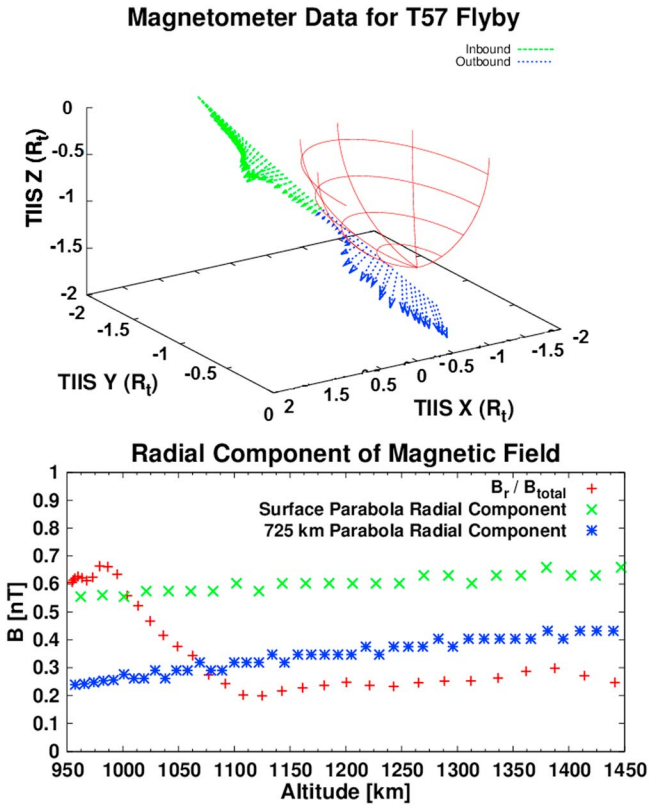

Figure 11. (top) Magnetometer data taken by the MAG instrument aboard Cassini during the T57 flyby. Titan is indicated in red, while the inbound (green) and outbound (blue) field vectors are indicated with arrows. Magnetic field components are given in Titan Ionospheric Interaction System (TIIS) coordinates. In TIIS coordinates, the *x* axis is in the direction of ideal corotation flow and the *y* direction is toward Saturn. Closest approach is on Titan's nightside. (bottom) The ratio of the radial component to the total magnitude of the magnetic field and the radial components of parabolic magnetic field lines anchored at Titan's surface and at an altitude of 725 km are also shown.

The CH_3^+ density profile produced by the full photochemical model with the surface-anchored parabolic field line agrees best with the measured INMS density profile between 1130 and 1350 km (Figure 12). In particular, the peak CH_3^+ densities agree well. But below 1100 km, better agreement with data is obtained with a parabolic magnetic field line anchored at 725 km (that is, more horizontal, or highly draped, magnetic field). As the magnetometer observed larger radial components of the magnetic field near closest approach (Figure 11), which is consistent with a parabolic magnetic field line anchored at the surface of Titan, this could indicate a modest attenuation. Overall, the model generates reasonable primary ionization rates (i.e., N_2^+ production rates) and, unlike *Cravens et al.* [2009b], *Gronoff et al.* [2009b], or *Agren et al.* [2007] for T5, without requiring attenuation of the magnetospheric electron fluxes from their full magnetospheric values.

Figure 13 shows the empirical N_2^+ production rate derived from CH_3^+ and CH_4 densities measured by INMS for T57. For comparison, the production rate from the full model is shown for the surface-anchored parabola case and 725 km anchored parabola case.

Primary production of CH_4^+ from electron impact ionization of methane was also calculated for T57. Again, the modeled and INMS-measured densities of CH_4^+ agree best for the surface-anchored parabola case above 1150 km and the 725 km anchored parabola case below 1140 km. The modeled densities of CH_4^+ are within 20% of the measured values. Figure 14 shows the empirical primary CH_4^+ production rates derived from densities of CH_4^+ and CH_4 measured by INMS.

3.3. Generic Nightside Ion Production Rates for Different Inputs

In this section the full two-stream plus chemical model is used to generate ion production rate profiles for all four "Rymer cases" [*Rymer et al.*, 2009] for the magnetospheric electron populations and for all the magnetic field configurations. The global average neutral density model presented in Paper 1 is used. No attenuation of magnetospheric electron fluxes (Figure 2) is assumed. Electron fluxes are shown for the following cases: (1) lobe like from the T8 flyby, (2) plasma sheet from the T13 flyby, (3) bimodal from the T31 flyby, and (4) magnetosheath from the T32 flyby. The results are shown in Figure 15 for N_2^+ production and in Figure 16 for CH_4^+ production resulting from electron impact ionization. Table 1 shows relative production rates of the other ion species produced by electron impact so that the results of Figures 15 and 16 can be extended to other primary ion species. Note that these branching ratios for the ionization products are rather insensitive to electron energies above about 20–30 eV or so (Table 1). These energies are above the ionization threshold for these products and do not affect their relative production rates.

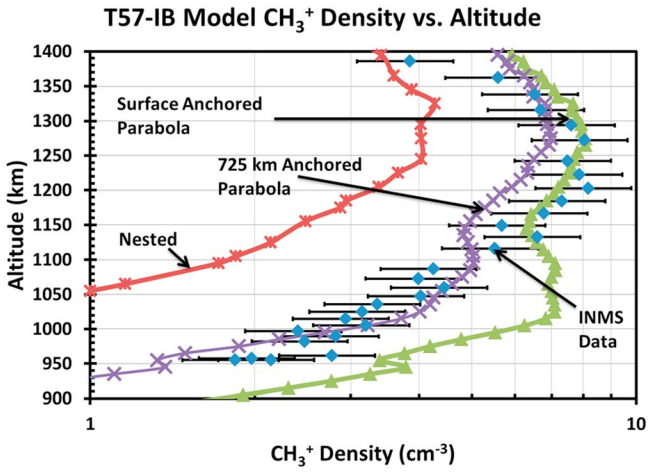

Figure 12. CH_3^+ density produced by the full photochemical model with magnetic field line topologies of a parabola anchored at the surface of Titan (green triangles), a parabola anchored at 725 km (purple crosses), and nested parabola (red stars) using the T57 magnetospheric electron flux measured by CAPS-ELS [*Kliore et al.*, 2011] as an input (Figure 10) compared to INMS data from the T57-Outbound flyby of Titan. INMS data are indicated with the blue diamonds. Note that although the surface-anchored parabola is more favored above 1100 km, the 725 km parabola appears to give better agreement below that altitude.

Figures 15 and 16 illustrate that, in general, higher-energy electrons penetrate deeper into the ionosphere generating ion production at lower altitudes. This is why the lobe-like, plasma sheet, and bimodal electron flux cases produce production rate profiles peaking at lower altitudes in comparison with the lower energy electrons from the magnetosheath. Higher-energy electrons also produce secondary electrons that can generate further ionization, and obviously, higher incident electron fluxes result in higher ion production rates.

As illustrated earlier for T5 and T57, the magnetic field line topology is also important in determining where incident electrons will deposit their energy [cf. *Galand et al.*, 2010; *Gronoff et al.*, 2009b; *Robertson et al.*, 2009; *Richard et al.*, 2011]. In general, the nested magnetic field line case, horizontal magnetic field lines, produces peak production rates 8–10 times lower than the parabola anchored at 725 km and 20–30 times lower than the radial magnetic field line. The peak altitude of the production rates generated with the nested magnetic field line is between approximately 150 (200) km higher than the peak altitude obtained with the parabolic magnetic field line anchored at 725 km (radial magnetic field line) for the lobe, bimodal, and plasma sheet cases and 200 (300) km higher for the magnetosheath case. These results are to be expected as the lower energy electrons more readily impact the neutral ions, and thus, the flux will decay more rapidly than that of a higher-energy electron population moving through the same amount of atmosphere.

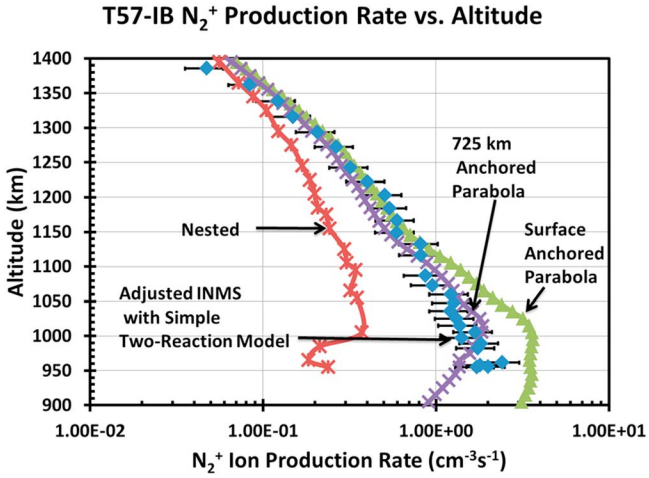

Figure 13. Modeled photoionization production rates of N_2^+ with magnetic field line topologies of a parabola anchored at the surface of Titan (green triangles), a parabola anchored at 725 km (purple crosses), and nested parabola (red stars) compared to the production rate of N_2^+ derived from INMS data using a simple two-reaction model adjusted by dividing the loss rate of CH_3^+ via reaction with methane by the branching factor shown in Figure 6 (blue diamonds) for the inbound leg of the T57 flyby of Titan.

Jagged peaks appear in radial cases in Figure 15. This is an artifact of the model resolution as the radial field line model has a resolution of 35 km where the nested and parabolic magnetic field line geometries have 10 km altitude resolution.

The shapes of the production rate profiles of CH_4^+ are similar to those of N_2^+ (Figure 16). The production rate profiles generated in this section can be used in conjunction with the production rate profiles for the solar cases in order to create generic ion production profiles for a variety of solar zenith angles and magnetospheric electron conditions.

3.4. Empirical Production Rates for Other Nightside Flybys

Other than T5 and T57, other nightside Titan flybys we examined with INMS ion and neutral data suitable for obtaining empirical ion production rates are T26, T32, T36, T50, and T51. The N_2^+ empirical

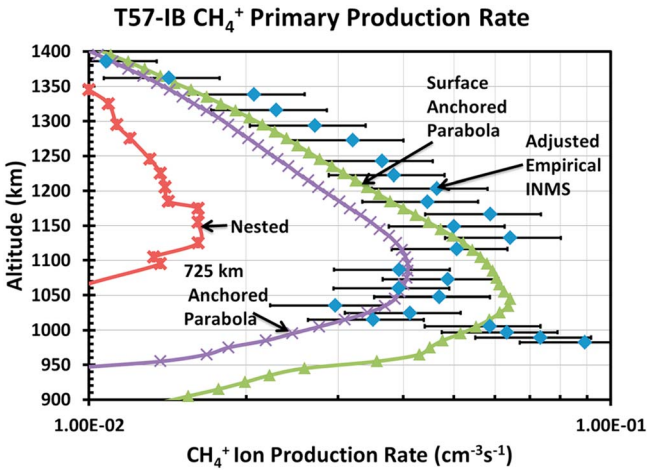

Figure 14. Modeled production rates of CH_4^+ with magnetic field line topologies of a parabola anchored at the surface of Titan (green triangles), a parabola anchored at 725 km (purple crosses), and nested parabola (red stars) using the full photochemical model compared to the empirical production rate of CH_4^+ derived from INMS data (blue diamonds) calculated by dividing the loss rate of CH_4^+ via reaction with methane by the branching ratio shown in Figure 6 for the T57-Inbound flyby of Titan.

production rates, organized according to plasma sheet, lobe-like, and bimodal nightside flybys, are shown in Figure 17 using equation (1) and an adjustment factor of 0.67 from Paper I [*Richard et al.*, 2015] and Figure 6 in the current paper to account for the amount of N_2^+ that does not react to form CH_3^+. Only deep nightside flybys containing INMS data are included, which is why there is not a curve for the lobe-like electron flux. The error bars represent the uncertainties in the production rates associated with the measured CH_3^+ and CH_4 densities. Comparison of Figures 15 and 17 confirms that the modeled electron precipitation reasonably represents the empirical production rates in shape and magnitude; however, for the plasma sheet and magnetosheath cases, radial field line topology must be used. Also, the theoretical electron impact production rates are falling short of the empirical production rates below altitudes of about 1050 km. Perhaps there is a missing, nonelectron precipitation, ionization source such as energetic ion precipitation [e.g., *Cravens et al.*, 2008; *Edberg et al.*, 2013; *Sillanpaa and Johnson*, 2013] or ion transport from the dayside for the case of longer-lived ions [*Cui et al.*, 2010].

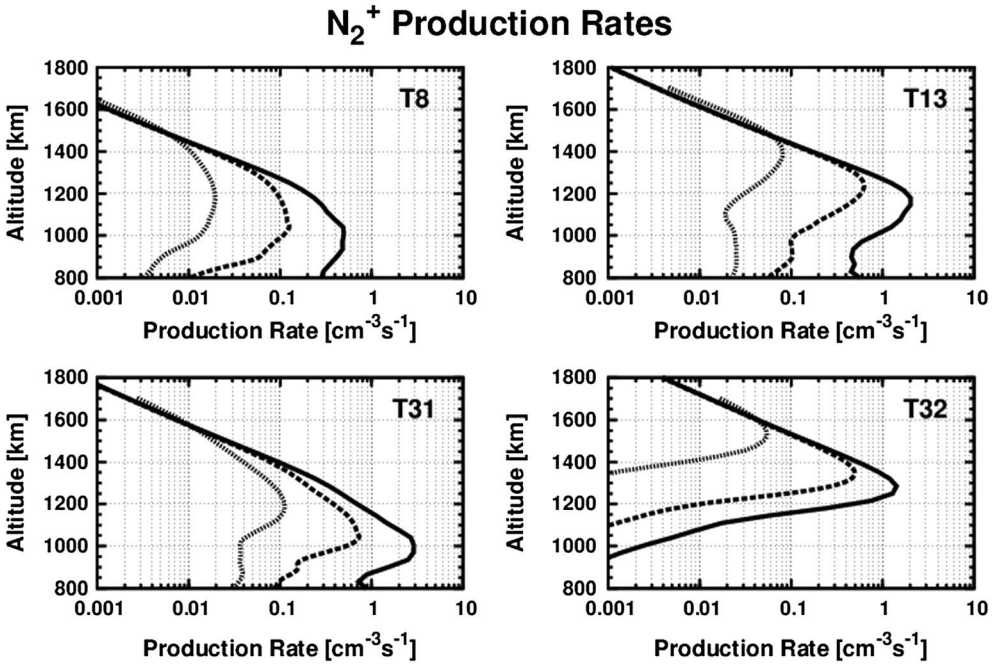

Figure 15. Production of N_2^+ using nested (dotted grey), parabolic (dashed), and radial (solid) magnetic field lines and the magnetospheric electron fluxes of the *Rymer et al.* [2009] classifications. Results are shown for model runs using the T8 lobe-like, T13 plasma sheet, T31 bimodal, and the T32 magnetosheath electron fluxes measured by CAPS-ELS. The magnetospheric electron flux profiles are shown in Figure 2.

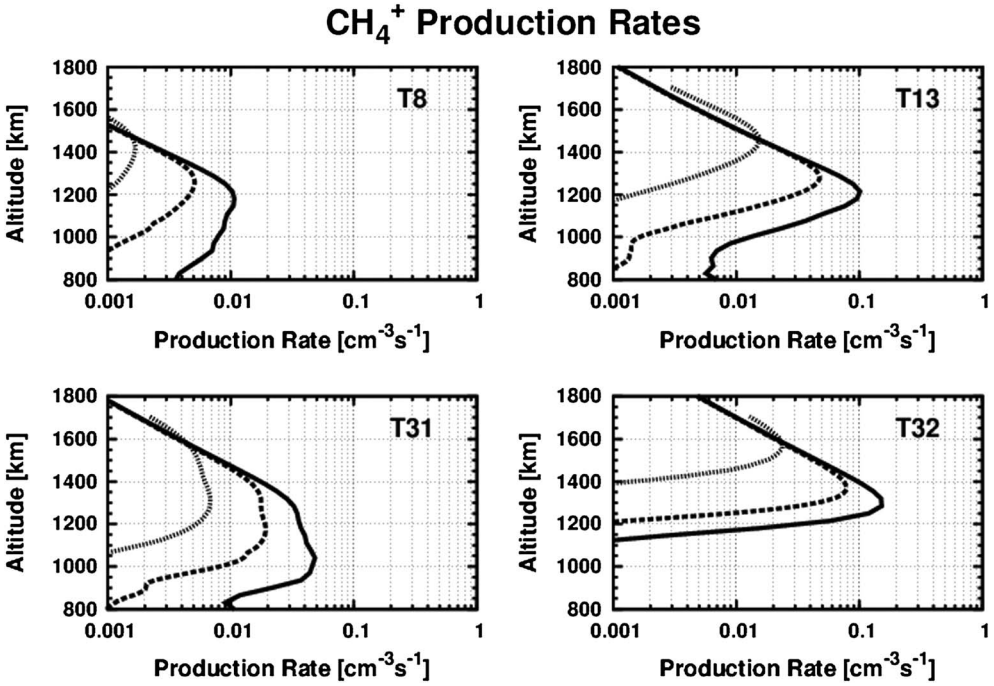

Figure 16. Primary production of CH_4^+ using nested (dotted grey), parabolic (dashed), and radial (black) magnetic field lines and the magnetospheric electron fluxes of the *Rymer et al.* [2009] classifications. Results are shown for model runs using the T8 lobe-like, the T13 plasma sheet, the T31 bimodal, and the T32 magnetosheath electron fluxes measured by CAPS-ELS. The magnetospheric electron flux profiles are shown in Figure 2.

4. Discussion

The model N_2^+ production rates agree well with the empirical INMS production rates for the surface parabola case for the T5 flyby at all altitudes except between 1175 and 1300 km, where model production rates exceed empirical rates by a factor of 2–3. The surface parabola magnetic field configuration gives a magnetic field orientation that agrees with Cassini magnetometer data. Figure 18 shows our electron impact-based model results for $HCNH^+$, $C_2H_5^+$, and the thermal electron density for T5. Just as on the dayside, the modeled densities of these major species are too high, even though the primary production rates are fine, leading to the conclusion that the model is missing chemical sinks. Similar comparisons for other flybys (e.g., T57) lead to the same conclusions.

For T57, the agreement of our model N_2^+ production rates with the INMS empirical production rates is good above an altitude of 1125 km, particularly with the surface parabola magnetic field model (i.e., the less draped magnetic field). But the surface parabola model ion production rates become a factor of 2 too large below 1125 km, and the 725 km parabola model (more draped field lines) provides better agreement.

For T57, the orientation of the measured magnetic field agrees overall with the surface parabola for higher altitudes. However, at lower altitudes the measured field has a large radial component, whereas the more highly draped magnetic field model was in better agreement with empirical production rates, which is puzzling.

Table 1. Ratios of Minor Ion Primary Production Rate to Major Ion Primary Production Rate at the Ionospheric Peak due to Electron Impact

Flyby	Altitude (km)	N^+ to N_2^+	CH_3^+ to CH_4^+	CH_2^+ to CH_4^+	CH^+ to CH_4^+	H_2^+ to CH_4^+	H^+ to CH_4^+
T8	1045	0.262	0.758	0.124	0.055	0.080	0.126
T13	1025	0.228	0.765	0.141	0.066	0.056	0.156
T31	1045	0.257	0.758	0.125	0.055	0.080	0.128
T32	1355	0.155	0.748	0.134	0.061	0.088	0.118

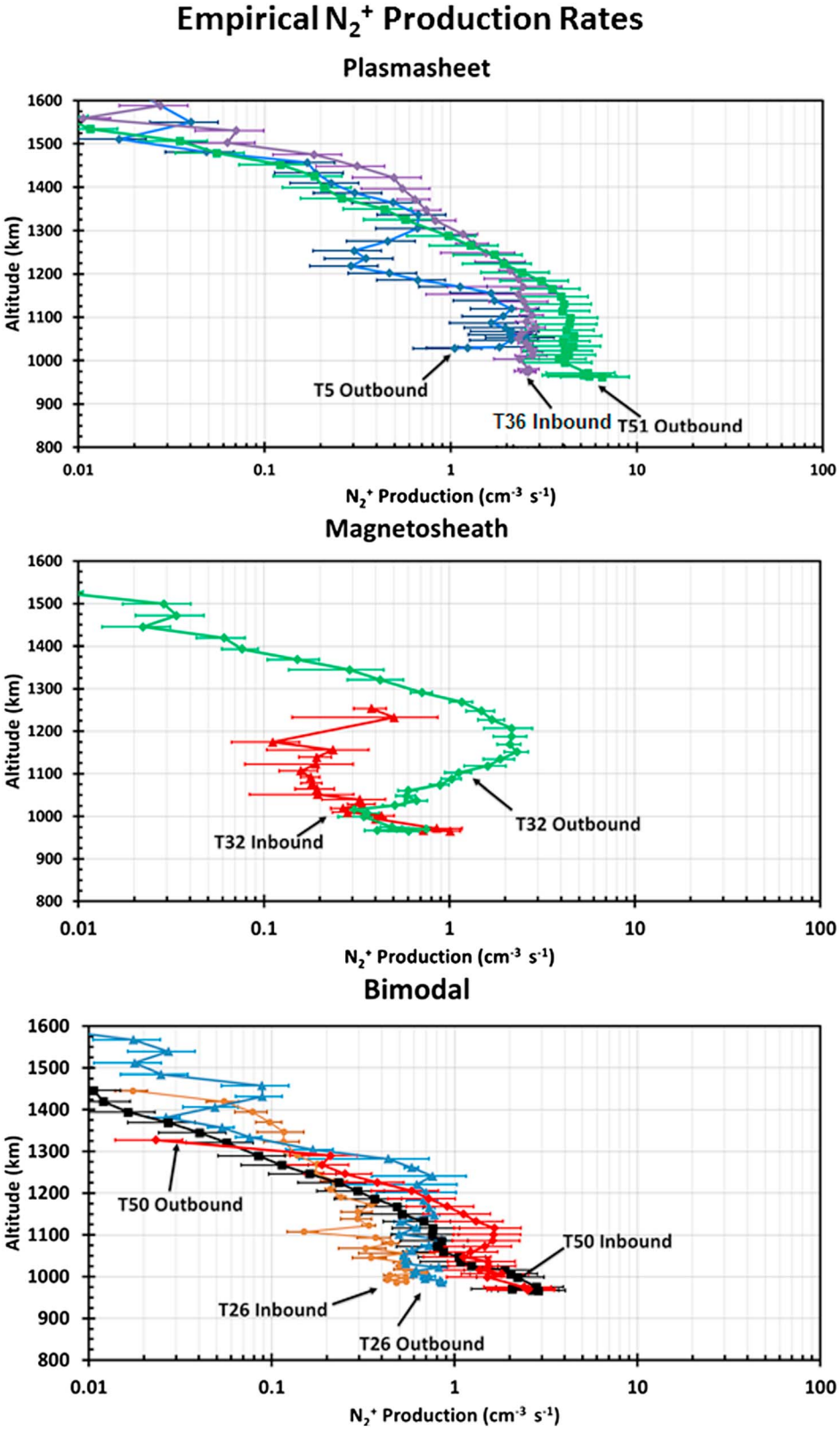

Figure 17. Empirical production rates for N_2^+ derived using the simple two-reaction model (equation (1)), INMS-measured densities, and an adjustment factor of 0.67. Production rates are generated for nightside flybys classified as (top) plasma sheet, (middle) magnetosheath, and (bottom) bimodal electron fluxes. Error bars represent uncertainties in INMS-measured densities.

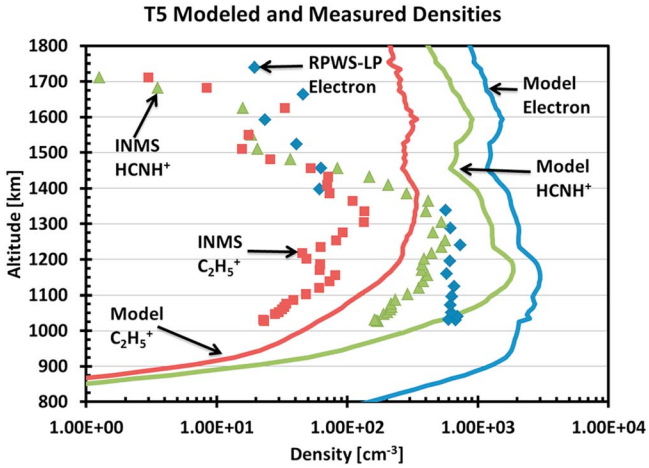

Figure 18. Comparisons between RPWS-LP measured (blue diamonds) and modeled electron densities (blue line) and INMS-measured (lines) and modeled densities of $HCNH^+$ (green triangles) and $C_2H_5^+$ (red squares).

As we discussed earlier in the paper, *Cravens et al*. [2009b] and *Agren et al*. [2007] assumed that the boundary electron fluxes into the electron transport model had to be reduced from fluxes in the outer magnetosphere by a factor of ≈ 10 in order to bring model electron densities into agreement with electron densities measured by the RPWS-LP or total ion density measured by INMS. As discussed earlier the suggestion was made that this attenuation is due to the electron content of a magnetic flux tube in Saturn's magnetosphere being depleted over time as it is "hung up" in Titan's ionosphere [cf. *Gan et al*., 1992; *Snowden et al*., 2013]. However, in the intervening time period, INMS neutral densities have increased by a factor of 2–3 [*Robertson et al*., 2009; *Westlake et al*., 2012; *Mandt et al*., 2012], affecting the model energy deposition, and there has been a growing recognition [*Galand et al*., 2014; *Westlake et al*., 2012; *Richard et al*., 2015] that photochemical models of Titan's ionosphere are missing loss processes for higher mass ion species.

The current paper's nightside ionosphere empirical ion production rate determinations (from INMS primary ion species) and model calculations indicate that factor of 10 magnetospheric electron flux attenuation is no longer needed. However, for the time period (or locations) on the outbound T5 pass, when Cassini was in the 1175–1300 km altitude range, a factor of 2–3 upper boundary electron flux reduction appears to be required, suggesting that at least for those flux tubes attenuation/depletion could be taking place. For T57, a large factor of 10 attenuation is not needed, but a factor of 2 incident electron flux attenuation would improve model-data comparisons in places. The model runs show that a more draped magnetic field configuration could accomplish this, but the measured magnetic field below 1125 km (Figure 11) is actually more radial (i.e., less draped), indicating that a factor of 2–3 electron flux attenuation is probably necessary for that time period (or location on Titan). It should be noted that negative ions also contribute to the overall charge density of the ionosphere [*Coates et al*., 2007a; *Ågren et al*., 2012; *Shebanits et al*., 2013; *Wellbrock et al*., 2013; *Vigren et al*., 2014].

Model-data comparisons in the current paper indicate that attenuation is not needed overall. If a major attenuation is no longer needed, the problem then becomes how to explain the overabundance of electrons in the models. An interesting feature in the ion densities measured by INMS during T5, first pointed out by *Cravens et al*. [2009b], has some bearing on this issue as mentioned earlier in the current paper (see the discussion in section 3.1). That is, the empirical production rates do show that in some locations there must be lower magnetospheric electron fluxes, perhaps due to the aforementioned attenuation. However, the chemically longer lived species (e.g., $HCNH^+$) show smoother profiles than do the primary species (Figure 18), indicating that time history of a flux tube is also important and also indicating that transport of ionospheric plasma from the dayside could be playing a role [*Cui et al*., 2010]. More work is needed on this topic.

5. Conclusions

In conclusion, the key findings of this study are the following:

1. Theoretically modeled electron-ion production rates are found to be within 25% of production rates derived empirically from INMS measurements for the T5 and the T57 nightside flybys of Titan.
2. The cause of the discrepancy between modeled and measured (data taken by INMS, RSS, and RPWS-LP) electron and ion densities is not due to overproduction of the primary ion species and therefore must be caused by insufficient electron-ion recombination.

3. Attenuation of the magnetospheric electron fluxes to the extent proposed by *Agren et al.* [2007] and *Cravens et al.* [2009b] is not needed to reproduce the primary production rates of the primary ion species on the nightside of Titan, although *Snowden et al.* [2013] have shown that flux tube erosion can lower ionization rates below 1300 km. If there is a large attenuation to the electron flux, additional ionization sources (i.e., ion precipitation) may be responsible.
4. Globally averaged ion production profiles have been generated for the ionization products of N_2 and CH_4 resulting from magnetospheric electron precipitation using the magnetospheric electron conditions described by *Rymer et al.* [2009] for a radial, a nested, and a parabolic magnetic field line anchored at 725 km. These production rates can be combined with the solar zenith angle-dependent production rates shown in Paper I to account for various conditions of Titan's ionosphere.
5. Empirical production rates have been derived from INMS measurements on the nightside of Titan for the plasma sheet, bimodal, and magnetosheath superthermal electron fluxes. These indicate that electron precipitation from the external plasma environment can account for most of the nightside ionosphere (and perhaps make a contribution on the dayside ionosphere, although it would be hard to observe due to large solar photoionization rates). However, our results show that below 1050 km or so, ionization by another source (i.e., ion precipitation) might be needed and that transport of plasma from the dayside could also be important for longer-lived ion species [cf. *Cui et al.*, 2010].

Acknowledgments

All Cassini data, including INMS data, are or will soon be available through the Planetary Data System. The research described in this paper was supported by the University of Kansas by NASA Cassini grant NA57-03001 via subcontract from the Southwest Research Institute and by NASA Planetary Atmospheres grant NNX10AB86G.

Michael Liemohn thanks the reviewers for their assistance in evaluating this paper.

References

Agren, K., et al. (2007), On magnetospheric electron impact ionization and dynamics in Titan's ram-side and polar ionosphere—A Cassini case study, *Ann. Geophys.*, *25*, 2359–2369.

Ågren, K., N. J. T. Edberg, and J.-E. Wahlund (2012), Detection of negative ions in the deep ionosphere of Titan during the Cassini T70 flyby, *Geophys. Res. Lett.*, *39*, L10201, doi:10.1029/2012GL051714.

Anicich, V. (2003), An index of the literature for bimolecular gas phase cation-molecule reaction kinetics, JPL Publ., 03–19.

Anicich, V., and M. McEwan (1997), Ion-molecule chemistry in Titan's ionosphere, *Planet. Space Sci.*, *45*(8), 897–921.

Arridge, C. S., N. Achilleos, M. K. Dougherty, K. K. Khurana, and C. T. Russell (2006), Modeling the size and shape of Saturn's magnetopause with variable dynamic pressure, *J. Geophys. Res.*, *111*, A11227, doi:10.1029/2005JA011574.

Arridge, C. S., N. André, N. Achilleos, K. K. Khurana, C. L. Bertucci, L. K. Gilbert, G. R. Lewis, A. J. Coates, and M. K. Dougherty (2008), Thermal electron periodicities at 20RS in Saturn's magnetosphere, *Geophys. Res. Lett.*, *35*, L15107, doi:10.1029/2008GL034132.

Banaskiewicz, M., L. M. Lara, R. Rodrigo, J. J. Lopez-Moreno, and G. J. Molina-Cuberos (2000), A coupled model of Titan's atmosphere and ionosphere, *Icarus*, *147*, 386–404.

Bertucci, C., et al. (2008), The magnetic memory of Titan's ionized atmosphere, *Science*, *321*, 1475–1478, doi:10.1126/science.1159780.

Bertucci, C., N. B. Sinclair, N. Achilleos, P. Hunt, M. K. Dougherty, and C. S. Arridge (2009), The variability of Titan's magnetic environment, *Planet. Space Sci.*, *57*, 1813–1820, doi:10.1016/j.pss.2009.02.009.

Bird, M. K., R. Dutta-Roy, S. W. Asmar, and T. A. Rebold (1997), Detection of Titan's ionosphere from Voyager 1 radio occultation observations, *Icarus*, *130*, 426–436.

Brescansin, L. M., M. A. P. Lima, and V. Mckoy (1989), Cross sections for rotational excitation of CH_4 by 3–20 eV electrons, *Phys. Rev. A*, *40*(10), 5577.

Carbary, J. F., and S. M. Krimigis (1982), Charged particle periodicity in the Saturnian magnetosphere, *Geophys. Res. Lett.*, *9*, 1073–1076, doi:10.1029/GL009i009p01073.

Carbary, J. F., D. G. Mitchell, S. M. Krimigis, D. C. Hamilton, and N. Krupp (2007), Charged particle periodicities in Saturn's outer magnetosphere, *J. Geophys. Res.*, *112*, A06246, doi:10.1029/2007JA012351.

Cartwright, D. C., S. Trajmar, A. Chutjian, and W. Williams (1977), Electron impact excitation of the electronic states of N_2. II: Integral cross sections at incident energies from 10 to 50 eV, *Phys. Rev. A*, *16*, 1041.

Coates, A. J., F. J. Crary, D. T. Young, K. Szego, C. S. Arridge, Z. Bebesi, and E. C. Sittler Jr. (2007a), Ionospheric electrons in Titan's tail: Plasma structure during the Cassini T9 encounter, *Geophys. Res. Lett.*, *34*, L24505, doi:10.1029/2007GL030919.

Coates, A. J., F. J. Crary, G. R. Lewis, D. T. Young, J. H. Waite Jr., and E. C. Sittler Jr. (2007b), Discovery of heavy negative ions in Titan's ionosphere, *Geophys. Res. Lett.*, *34*, L22103, doi:10.1029/2007GL30978.

Cravens, T., et al. (2006), Composition of Titan's ionosphere, *Geophys. Res. Lett.*, *33*, L07105, doi:10.1029/2005GL025575.

Cravens, T. E., J. Vann, J. Clark, J. Yu, C. N. Keller, and C. Brull (2004), The ionosphere of Titan: An updated theoretical model, *Adv. Space Res.*, *33*, 212–215.

Cravens, T. E., et al. (2005), Titan's ionosphere: Model comparisons with Cassini Ta data, *Geophys. Res. Lett.*, *32*, L12108, doi:10.1029/2005GL023249.

Cravens, T. E., I. P. Robertson, S. A. Ledvina, D. Mitchell, S. M. Krimigis, and J. H. Waite Jr. (2008), Energetic ion precipitation at Titan, *Geophys. Res. Lett.*, *35*, L03103, doi:10.1029/2007GL032451.

Cravens, T. E., R. V. Yelle, J.-E. Wahlund, D. E. Shemansky, and A. F. Nagy (2009a), Composition and structure of the ionosphere and thermosphere, in *Titan from Cassini-Huygens*, edited by R. H. Brown, J.-P. Lebreton, and J. H. Waite Jr., pp. 259–296, Springer, New York.

Cravens, T. E., et al. (2009b), Model-data comparisons for Titan's nightside ionosphere, *Icarus*, *199*, 174.

Cravens, T. E., et al. (2010), Dynamical and magnetic field time constants for Titan's ionosphere: Empirical estimates and comparisons with Venus, *J. Geophys. Res.*, *115*, A08319, doi:10.1029/2009JA015050.

Cui, J., et al. (2009), Analysis of Titan's neutral upper atmosphere from Cassini Ion Neutral Mass Spectrometer measurements, *Icarus*, *200*, 581.

Cui, J., M. Galand, R. V. Yelle, J.-E. Wahlund, K. Ågren, J. H. Waite Jr., and M. K. Dougherty (2010), Ion transport in Titan's upper atmosphere, *J. Geophys. Res.*, *115*, A06314, doi:10.1029/2009JA014563.

Edberg, N. J. T., et al. (2013), Extreme densities in Titan's ionosphere during the T85 magnetosheath encounter, *Geophys. Res. Lett.*, *40*, 2879–2883, doi:10.1002/grl.50579.

Edwards, S., C. Freeman, and M. McEwan (2008), The ion chemistry of methylenimine and propionitrile and their relevance to Titan, *Int. J. Mass Spectrom.*, *272*(1), 86–90.

Fulchignoni, M., et al. (2005), In situ measurements of the physical characteristics of Titan's environment, *Nature*, *438*, 785–791.
Galand, M., J. Lilensten, D. Toublanc, and S. Maurice (1999), The ionosphere of Titan: Ideal diurnal and nocturnal cases, *Icarus*, *140*, 92–105.
Galand M., R. Yelle, J. Cui, J.-E. Wahlund, V. Vuitton, A. Wellbrock, and A. Coates (2010), Ionization sources in Titan's deep ionosphere, *J. Geophys. Res.*, *115*, A07312, doi: 10.1029/2009JA015100.
Galand, M., A. Coates, T. Cravens, and J.-E. Wahlund (2014), Titan's ionosphere, in *Titan: Interior, Surface, Atmosphere, and Space Environment*, edited by I. C. F. Mueller-Wodarg et al., pp. 376–418, Cambridge Univ. Press, New York.
Gan, L., C. N. Keller, and T. E. Cravens (1992), Electrons in the ionosphere of Titan, *J. Geophys. Res.*, *97*, 12,136–12,151.
Gan, L., T. E. Cravens, and C. N. Keller (1993), A time-dependent model of suprathermal electrons at Titan, in *Plasma Environments of Non-Magnetic Planets*, vol. 4, edited by T. I. Gombosi, 171 pp., Elsevier, Oxford, U. K.
Green, A. E. S., and S. K. Dutta (1967), Semi-empirical cross sections for electron impacts, *J. Geophys. Res.*, *72*, 3933–3941, doi:10.1029/JZ072i015p03933.
Green, A. E. S., and T. Sawada (1972), Ionization cross sections and secondary electron distributions, *J. Atmos. Sol. Terr. Phys.*, *34*, 1719.
Green, A. E. S., and R. S. Stolarski (1972), Analytic models of electron impact excitation cross sections, *J. Atmos. Sol. Terr. Phys.*, *34*, 1703–1717.
Gronoff, G., J. Lilensten, L. deSorgher, and E. Fluckiger (2009a), Ionization processes in the atmosphere of Titan I. Ionization in the whole atmosphere, *Astron. Astrophys.*, *506*, 955–964.
Gronoff, G., J. Lilensten, and R. Modolo (2009b), Ionization processes in the atmosphere of Titan II. Electron precipitation along magnetic field lines, *Astron. Astrophys.*, *506*, 965–970.
Hartle, R. E., E. C. Sittler Jr., K. Ogilvie, J. D. Scudder, A. J. Lazarus, and S. K. Atreya (1982), Titan's ion exosphere observed from Voyager 1, *J. Geophys. Res.*, *87*, 1383–1394, doi:10.1029/JA087iA03p01383.
Itikawa, I. (2006), Cross sections for electron collisions with nitrogen molecules, *J. Phys. Chem. Ref. Data*, *35*, 31–53.
Jain, A. (1986), Total (elastic + absorption) cross sections for e-CH_4 collisions in a spherical model at 0.10–500 eV, *Phys. Rev. A*, *34*(5), 3707.
Jain, A., and D. G. Thompson (1983), Rotational excitation of CH_4 and H_2O by slow electron impact, *J. Phys. B: At. Mol. Phys.*, *16*, 3077.
Keller, C. N., T. E. Cravens, and L. Gan (1992), A model of the ionosphere of Titan, *J. Geophys. Res.*, *97*, 12,117–12,135, doi:10.1029/92JA00231.
Keller, C. N., V. G. Anicich, and T. E. Cravens (1998), Model of Titan's ionosphere with detailed hydrocarbon chemistry, *Planet. Space Sci.*, *46*, 1157–1174.
Kliore, A. J., et al. (2008), First results from the Cassini radio occultations of the Titan ionosphere, *J. Geophys. Res.*, *113*, A09317, doi:10.1029/2007JA012965.
Kliore, A. J., A. F. Nagy, T. E. Cravens, M. S. Richard, and A. M. Rymer (2011), Unusual electron density profiles observed by Cassini radio occultations in Titan's ionosphere: Effects of enhanced magnetospheric electron precipitation?, *J. Geophys. Res.*, *116*, A11318, doi:10.1029/2011JA016694.
Krasnopolsky, V. (2009), A photochemical model of Titan's atmosphere and ionosphere, *Icarus*, *201*, 226–256.
Lavvas, P., M. Galand, R. V. Yelle, A. N. Heays, B. R. Lewis, G. R. Lewis, and A. J. Coates (2011), Energy deposition and primary chemical products in Titan's upper atmosphere, *Icarus*, *213*, 233–251, doi:10.1016/j.icarus.2011.03.001.
Lavvas, P. P., A. Coustenis, and I. M. Vardavas (2008a), Coupling photochemistry with haze formation in Titan's atmosphere. Part I. Model description, *Planet. Space Sci.*, *56*, 27–66.
Lavvas, P. P., A. Coustenis, and I. M. Vardavas (2008b), Coupling photochemistry with haze formation in Titan's atmosphere. Part II. Results and validation with Cassini/Huygens data, *Planet. Space Sci.*, *56*, 67–99.
Ledvina, S. A., S. H. Brecht, and T. E. Cravens (2012), The orientation of Titan's dayside ionosphere and its effects on Titan's plasma interaction, *Earth Planets Space*, *64*, doi:10.5047/eps.2011.08.009.
Lewis, G. R., N. Andre, C. S. Arridge, A. J. Coates, L. K. Gilbert, D. R. Linder, and A. M. Rymer (2008), Derivation of density and temperature from the Cassini-Huygens CAPS electron spectrometer, *Planet. Space Sci.*, *56*, 901–912, doi:10.1016/j.pss.2007.12.017.
Lilensten, J., O. Witasse, C. Simon, H. Soldi-Lose, O. Dutuit, R. Thissen, and C. Alcaraz (2005a), Prediction of a N++ 2 layer in the upper atmosphere of Titan, *Geophys. Res. Lett.*, *32*, L03203, doi:10.1029/2004GL021432.
Lilensten, J., C. Simon, O. Witasse, O. Dutuit, R. Thissen, and C. Alcarez (2005b), A fast comparison of the diurnal secondary ion production in the ionosphere of Titan, *Icarus*, *174*, 285–288.
Lindsay, B. G., and M. A. Mangan (2003), Cross sections for ion production by electron collision with molecules, in *Landolt-Börnstein, Photon- and Electron-Interaction With Molecules: Ionization and Dissociation, New. Ser.*, vol. I/17C, edited by Y. Itikawa, pp. 5-1–5–77, Springer, New York.
Liu, X., and D. E. Shemansky (2006), Analysis of electron impact ionization properties of methane, *J. Geophys. Res.*, *111*, A04303, doi:10.1029/2005JA011454.
Ma, Y., A. F. Nagy, T. E. Cravens, I. V. Sokolov, K. C. Hansen, J.-E. Wahlund, F. J. Crary, A. J. Coates, and M. K. Dougherty (2006), Comparisons between MHD model calculations and observations of Cassini flybys of Titan, *J. Geophys. Res.*, *111*, A05207, doi:10.1029/2005JA011481.
Ma, Y.-J., et al. (2009), Time-dependent global MHD simulations of Cassini T32 flyby: From magnetosphere to magnetosheath. *J. Geophys. Res.*, *114*, A03204, doi:10.1029/2008JA013676.
Magee, B., J. Bell, J. H. Waite Jr., K. Mandt, J. Westlake, and D. Gell (2009), INMS derived composition of Titan's upper atmosphere: Analysis methods and model comparison, *Planet. Space Sci.*, *57*, 1895–1916.
Mandt, K. E., et al. (2012), Ion densities and composition of Titan's upper atmosphere derived from the Cassini Ion Neutral Mass Spectrometer: Analysis methods and comparison of measured ion densities to photochemical model simulations, *J. Geophys. Res.*, *117*, E10006, doi:10.1029/2012JE004139.
McEwan, M. J., and V. G. Anicich (2007), Titan's ion chemistry: A laboratory perspective, *Mass Spectrom. Rev.*, *26*, 281–319.
Molina-Cuberos, G. J., H. Lammer, W. Stumptner, K. Schwingenschuh, H. O. Rucker, J. J. Lopez-Moreno, K. Rodrigo, and T. Tokano (2001), Ionosphere layer induced by meteoric ionization in Titan's atmosphere, *Planet. Space Sci.*, *49*, 143–153.
Muller, R., K. Jung, K.-H. Kochem, W. Sohn, and H. Ehrhardt (1985), Rotational excitation of CH_4 by low-energy-electron collisions, *J. Phys. B: At. Mol. Phys.*, *18*, 3971.
Nagy, A. F., and P. M. Banks (1970), Photoelectron fluxes in the ionosphere, *J. Geophys. Res.*, *75*, 6260–6270, doi:10.1029/JA075i031p06260.
Neubauer, F. M., D. A. Gurnett, J. D. Scudder, and R. E. Hartle (1984), Titan's magnetospheric interaction, in *Saturn*, edited by T. Gehrels and M. D. Matthews, pp. 760–787, Univ. of Ariz. Press, Tucson.
Porter, H. S., C. H. Jackman, and A. E. S. Green (1976), Efficiencies for production of atomic nitrogen and oxygen by relativistic proton impact in air, *J. Chem. Phys.*, *65*, 154.
Richard, M. S., T. E. Cravens, I. P. Robertson, J. H. Waite, J.-E. Wahlund, F. J. Crary, and A. J. Coates (2011), Energetics of Titan's ionosphere: Model comparisons with Cassini data, *J. Geophys. Res.*, *116*, A09310, doi:10.1029/2011JA016603.
Richard, M. S., et al. (2015), An empirical approach to modeling ion production rates in Titan's ionosphere I: Ion production rates on the dayside and globally, *J. Geophys. Res. Space Physics*, doi:10.1002/2013JA019706.

Robertson, I. P., et al. (2009), Structure of Titan's ionosphere: Model comparisons with Cassini data, *Planet. Space Sci.*, *57*, 1834, doi:10.1016/j.pss.2009.07.011.
Rohr, K. (1980), Cross beam experiment for the scattering of low-energy electrons from methane, *J. Phys. B: At. Mol. Phys.*, *13*, 4897.
Rymer, A. M., H. T. Smith, A. Wellbrock, A. J. Coates, and D. T. Young (2009), Discrete classification and electron energy spectra of Titan's varied magnetospheric environment, *Geophys. Res. Lett.*, *36*, L15109, doi:10.1029/2009GL039427.
Schunk, R. W., and A. F. Nagy (2009), *Ionospheres*, 2nd ed., Cambridge Univ. Press, Cambridge, U. K.
Sergis, N., S. M. Krimigis, D. G. Mitchell, D. C. Hamilton, N. Krupp, B. H. Mauk, E. C. Roelof, and M. K. Dougherty (2009), Energetic particle pressure in Saturn's magnetosphere measured with the Magnetospheric Imaging Instrument on Cassini, *J. Geophys. Res.*, *114*, A02214, doi:10.1029/2008JA013774.
Shebanits, O., J.-E. Wahlund, K. Mandt, K. Ågren, N. J. T. Edberg, and J. H. Waite Jr. (2013), Negative ion densities in the ionosphere of Titan-Cassini RPWS/LP results, *Planet. Space Sci.*, *84*, 153–162, doi:10.1016/j.pss.2013.05.021.
Shimamura, I. (1983), Partial-sum rules for and asymmetry between rotational transitions $J \pm \Delta J \leftarrow J$, *Phys. Rev. A*, *28*(3), 1357.
Sillanpaa, I., and R. Johnson (2013), The role of ion-neutral collisions in Titan's magnetospheric interaction, *J. Geophys. Res*.
Sittler, E. C., R. E. Hartle, C. Bertucci, A. Coates, T. E. Cravens, I. Dandouras, and D. E. Shemansky (2009), Energy deposition processes in Titan's upper atmosphere and its induced magnetosphere, in *Titan From Cassini-Huygens*, edited by R. H. Brown, J.-P. Lebreton, and J. H. Waite, pp. 393–454, Springer, New York.
Snowden, D., R. V. Yelle, M. Galand, A. J. Coates, A. Wellbrock, G. H. Jones, and P. Lavvas (2013), Auroral electron precipitation and flux tube erosion in Titan's upper atmosphere, *Icarus*, *226*(1), 186–204.
Sohn, W., K. Jung, and H. Ehrhardt (1983), Threshold structures in the cross section of low-energy electron scattering of methane, *J. Phys. B: At. Mol. Phys.*, *16*, 891.
Solomon, S. C., P. B. Hays, and V. J. Abreu (1988), The auroral 6300 Å emission: Observations and modeling, *J. Geophys. Res.*, *93*, 9867–9882, doi:10.1029/JA093iA09p09867.
Straub, H. C., D. Lin, B. G. Lindsay, K. A. Smith, and R. F. Stebbings (1997), Absolute partial cross sections for electron-impact ionization of CH_4 from threshold to 1000 eV, *J. Chem. Phys.*, *106*, 4430–4435.
Tabata, T., T. Shirai, M. Sataka, and H. Kubo (2006), Analytic cross sections for electron impact collisions with nitrogen molecules, *At. Data Nucl. Data Tables*, *92*, 375–406.
Tanaka, H., M. Kubo, N. Onodera, and A. Suzuki (1983), Vibrational excitation of CH_4 by electron impact: 3–20 eV, *J. Phys. B: At. Mol. Phys.*, *16*, 2861.
Trajmar, S., D. F. Register, and A. Chutjian (1983), Electron scattering by molecules: II. Experimental methods and data, *Phys. Rep. Rev. Sec. Phys. Lett.*, *97*, 219.
Ulusen, D., J. G. Luhmann, Y.-J. Ma, S. Ledvina, T. E. Cravens, K. Mandt, J. H. Waite, and J.-E. Wahlund (2010), Investigation of the force balance in the Titan ionosphere: Cassini T5 flyby model/data comparisons, *Icarus*, *210*, 867–880, doi:10.1016/j.icarus.2010.07.004.
Vigren, E., M. Galand, O. Shebanits, J.-E. Wahlund, W. D. Geppert, P. Lavvas, V. Vuitton, and R. V. Yelle (2014), Increasing positive ion number densities below the peak of ion-electron pair production in Titan's ionosphere, *Astrophs. J.*, *786*, 69, doi:10.1088/0004-637X/786/1/1.
Vuitton, V., R. V. Yelle, and V. G. Anicich (2006), The nitrogen chemistry of Titan's upper atmosphere revealed, *Astrophys. J.*, *647*, L175–L178.
Vuitton, V., R. V. Yelle, and M. McEwan (2007), Ion chemistry and N-containing molecules in Titan's upper atmosphere, *Icarus*, *191*, 722–742.
Vuitton, V., R. Yelle, and J. Cui (2008), Formation and distribution of benzene on Titan, *J. Geophys. Res.*, *113*, E05007, doi:10.1029/2007JE002997.
Vuskovic, L., and S. Trajmar (1983), Electron impact excitation of methane, *J. Chem. Phys.*, *78*, 4947.
Wahlund, J.-E., et al. (2005), Cassini measurements of cold plasma in the ionosphere of Titan, *Science*, *308*, 986–989.
Waite, J. H., Jr., et al. (2005), Ion Neutral Mass Spectrometer (INMS) results from the first flyby of Titan, *Science*, *308*, 982–986.
Waite, J. H., Jr., D. T. Young, T. E. Cravens, A. J. Coates, F. J. Crary, B. Magee, and J. Westlake (2007), The process of tholin formation in Titan's upper atmosphere, *Science*, *316*, 870–875.
Wellbrock, A., A. J. Coates, G. H. Jones, G. R. Lewis, and J. H. Waite (2013), Cassini CAPS-ELS observations of negative ions in Titan's ionosphere: Trends of density with altitude, *Geophys. Res. Lett.*, *40*, 4481–4485, doi:10.1002/grl.50751.
Westlake, J. H., J. H. Waite Jr., K. E. Mandt, N. Carrasco, J. M. Bell, B. A. Magee, and J.-E. Wahlund (2012), Titan's ionospheric composition and structure: Photochemical modeling of Cassini INMS data, *J. Geophys. Res.*, *117*, E01003, doi:10.1029/2011JE003883.
Wilson, E., and S. Atreya (2004), Current state of modeling the photochemistry of Titan's mutually dependent atmosphere and ionosphere, *J. Geophys. Res.*, *109*, E06002, doi:10.1029/2003JE002181.
Young, D. T., et al. (2005), Composition and dynamics of plasma in Saturn's magnetosphere, *Science*, *307*, 1262–1266.
Zabka, J., M. Polasek, D. Ascenzi, P. Tosi, and D. Schroder (2009), Reactivity of $C_2H_5^+$ with benzene: Formation of ethylbenzenium ions and implications for Titan's ionospheric chemistry, *J. Phys. Chem. A*, *113*(42), 11,153–11,160.
Zipf, E. C., and R. W. McLaughlin (1978), On the dissociation of nitrogen by electron impact and by E.U.V. photo-absorption, *Planet. Space Sci.*, *26*, 449.